Computer Physics Communications 137 (2001) 12–24

Computer Physics Communications

www.elsevier.nl/locate/cpc

Solving the structure completion problem in surface crystallography

D.K. Saldin [a,*], R. Harder [a], H. Vogler [b], W. Moritz [b], I.K. Robinson [c]

[a] *Department of Physics and Laboratory for Surface Studies, University of Wisconsin-Milwaukee, P.O. Box 413, Milwaukee, WI 53201, USA*

[b] *Institute for Crystallography and Mineralogy, University of Munich, Theresienstrasse 41, 80333 Munich, Germany*

[c] *Department of Physics, University of Illinois, Urbana, IL 61801, USA*

Abstract

Measured intensities of short-wavelength radiation diffracted from a crystal surface contain a contribution from the known bulk structure and the unknown surface structure. The recovery of the diffracted amplitude from the unknown surface from the experimental intensity measurements and from calculated amplitudes from the known bulk (treated as a reference wave) is closely analogous to holography, or to the structure completion problem in bulk crystallography. We show how an algorithm based on ideas of Bayesian statistics enables the direct recovery of the surface electron density from simulated surface X-ray diffraction data.

PACS: 61.10.Dp; 68.35.Bs

Keywords: Structure completion; Direct method; Holography; Bayesian statistics; Maximum entropy; Surface X-ray diffraction; Surface crystallography

1. Introduction

Traditional methods for surface crystallography have tended to be based on trial-and-error comparisons of model-based calculations of diffracted intensities of short-wavelength radiation with experimental data [1]. A physically reasonable model which gives rise to a good fit with the data is regarded as a likely model. As pointed out by Pendry et al. [2] there are serious limitations to the complexity of completely unknown structures that may be determined by such means. This is due to the rapid growth of the number of structures to be tested with the number of parameters to be determined. Consequently there has been an interest in developing direct methods for surface crystallography [2] that somehow avoid this unfortunate scaling with complexity.

One idea that has received significant attention in the last decade or so is the holographic interpretation of diffraction patterns from surfaces [3]. In photoelectron holography, an electron ejected from an atomic core due to absorption of an X-ray photon may be regarded as a diverging spherical *reference wave* source. The scattering of this wave by nearby atoms creates *object waves* diverging from those atoms coherent with the directly photoemitted wave. The angular and energy variation of the far-field interference pattern of these reference and object waves may be regarded as a hologram [4,5]. A back-propagation algorithm [6] en-

* Corresponding author.
E-mail address: dksaldin@uwm.edu (D.K. Saldin).

0010-4655/01/$ – see front matter
PII: S0010-4655(01)00169-2

ables the determination of the positions of nearby scattering atoms relative to the position of the reference-wave source. The holographic interpretation of other forms of diffraction patterns have also been proposed for the similar purpose of determining the 3D structure of a local cluster of atoms. Such techniques include holographic LEED [7], X-ray fluorescence holography [8], multiple-energy X-ray holography [9], etc.

A disadvantage of all these techniques for the determination of the entire structure of a large unknown unit cell is that, due to the inverse-square decay of the intensity of a spherical reference wave, it is usually the structure of only a rather small local cluster of atoms around the reference-wave source that may be determined. A recent example in point was the use of holographic LEED as an aid for the determination of the SiC(111)-(3×3) structure [10]. Holographic reconstruction was able to determine the structure of a local 5 atom cluster around a prominent adatom on the surface in a matter of hours, but the elucidation of the positions of the other atoms of the unit cell by conventional trial-and-error methods required a further half year.

In this paper we discuss a method which, in a sense, may also be thought of as holographic, but which promises the direct recovery of the structure of even a complicated entire surface unit cell, at least in the case of surface X-ray diffraction. The crucial point is to realize that when an external source of radiation is used as a diffraction probe for surface crystallography, the scattering of this radiation takes place not only from the unknown surface structure, but also from the known bulk structure. Indeed the total scattered amplitude may be regarded as a sum of these two contributions. If $I_{\mathbf{q}}$ represents the intensity of radiation scattered from a unit cell and which undergoes a momentum transfer $\mathbf{q}$, it may be written

$$I_{\mathbf{q}} = \left|F_{\mathbf{q}}^{\exp}\right|^2 = |B_{\mathbf{q}} + S_{\mathbf{q}}|^2, \tag{1}$$

where $F_{\mathbf{q}}^{\exp}$ represents the total structure factor from the experiment, $B_{\mathbf{q}}$ the contribution from the (known) bulk unit cell, and $S_{\mathbf{q}}$ that from the unknown surface unit cell. If the set of measurable intensities, $\{I_{\mathbf{q}}\}$, are considered to constitute a hologram, then $B_{\mathbf{q}}$ may be identified with a reference wave, and $S_{\mathbf{q}}$ with an object wave. If an algorithm may be devised for recovering the set $\{S_{\mathbf{q}}\}$ from $\{I_{\mathbf{q}}\}$ and $\{B_{\mathbf{q}}\}$ (the classic problem of holography [4,5]), at least in the case of (weakly scattered) X-rays, the recovery of the electron density of the entire surface unit cell is a relatively simple matter since it is related to the amplitudes $\{S_{\mathbf{q}}\}$ by a Fourier transform.

The idea of using a knowledge of part of a structure in combination with the measured diffraction data to find the rest of the structure is commonly exploited in protein crystallography, where it is known as the *structure completion problem* [11,12]. We point out that the problem of surface crystallography is intrinsically of the same kind since the measured diffraction data almost invariably has contributions from the known bulk structure.

We discuss strategies for the direct determination of the *surface* structure, with particular attention to surface X-ray diffraction (SXRD) [13] and describe a particularly promising algorithm. The outline of the rest of the paper is as follows: Section 2 contains an introduction to the technique of SXRD. In Section 3 we discuss one form of such an algorithm and point out some problems with it. Section 4 contains an introduction to the principles of Bayesian statistics which constitute a theoretical background for our method. Section 5 describes the particular implementation of these principles, known as the maximum entropy method, and our development of the method for the present application. Section 6 describes the results of applying our algorithm to a couple of test surface structures, and Section 7 contains a discussion and conclusions.

2. Surface X-ray diffraction

The technique of surface X-ray diffraction attempts to recover the structure of a surface from an analysis of the measured scattered amplitudes from a collimated beam of X-rays of glancing incidence. A reciprocal space diagram of the experimental geometry is shown in Fig. 1. The wavevector of X-rays (commonly of glancing incidence) is denoted by $\mathbf{k}_0$, and the wavevector of the detected beam is $\mathbf{k}$. Due to the 2D periodicity of the surface, the wavevector difference, $\mathbf{q} = \mathbf{k} - \mathbf{k}_0$ must join the reciprocal space origin (at the end of the wavevector $\mathbf{k}_0$) with the intersection of a rod specified by in-plane Miller indices (H, K) and the Ewald sphere (at out-of-plane Miller index value L). Thus the vector $\mathbf{q}$ may be specified by the three Miller indices (H, K, L). Although the

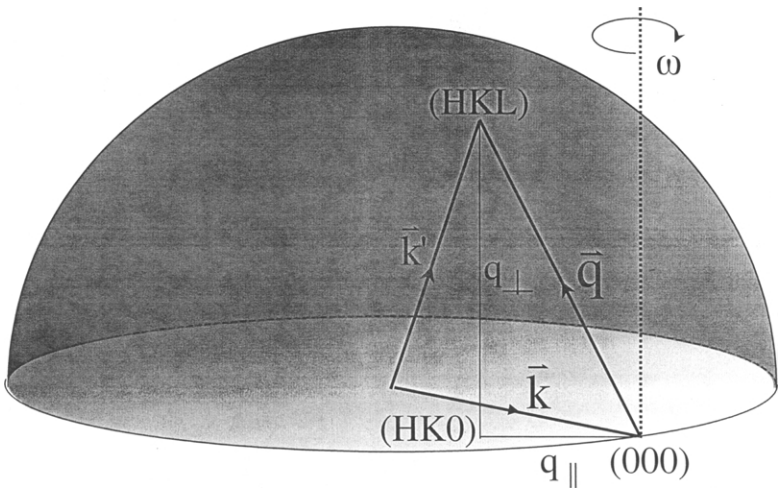

Fig. 1. Reciprocal space geometry of a surface X-ray diffraction experiment. The wavevector of the incident X-rays is represented by **k**; that of the diffracted beam by $\mathbf{k}'$. The wavevector difference, $\mathbf{q}(=\mathbf{k}'-\mathbf{k})$ joins the origin (000) to the intersection of the Ewald sphere with the (HKL) reciprocal lattice rod (H and K are discrete, but L is continuous).

2D periodicity restricts the H and K indices to discrete values, the lack of periodicity perpendicular to the surface allows non-zero diffracted intensity for arbitrary values of L, which may be varied by rotating the sample relative to the incident beam as shown. The intensity variation with L of the diffracted amplitudes corresponding to integer values of H and K (with respect to the substrate reciprocal lattice) is known as a crystal truncation rod (CTR).

The intensity of a beam corresponding to the scattered wavevector **q** is essentially the square modulus of the structure factor $F_{\mathbf{q}}^{\exp}$. Thus the *modulus* of the structure factor may be determined immediately from the measured data, but not its phase. If the phases of the structure factors were also known, a simple Fourier transform would recover the number, u_i, of electrons associated with position $\mathbf{r}_i$, of a uniform grid covering the slab representing the surface region, viz:

$$u_i = \frac{1}{N}\sum_{\mathbf{q}} \left(F_{\mathbf{q}}^{\exp} - B_{\mathbf{q}}\right) \exp(-\mathrm{i}\mathbf{q}.\mathbf{r}_i), \tag{2}$$

where $B_{\mathbf{q}}$ is the (known) diffracted amplitude from the bulk, and N the number of points i in the real-space grid. Given the lack of this phase information, a more sophisticated algorithm is required to recover the surface electron distribution.

3. Holographic method

The holographic method of Szöke [14,15] is one such technique. In X-ray diffraction the surface contribution to the structure factor may be written

$$S_{\mathbf{q}} = \sum_j u_j \exp(\mathrm{i}\mathbf{q}.\mathbf{r}_j). \tag{3}$$

Substituting (3) into (1), and equating the measured intensity $|F_{\mathbf{q}}^{\exp}|^2$ to its calculated counterpart yields

$$\left|F_{\mathbf{q}}^{\exp}\right|^2 - |B_{\mathbf{q}}|^2 = \sum_j u_j \left\{B_q^* M_{\mathbf{q},j} + \text{c.c.}\right\} + \sum_j \sum_l u_j u_l M_{\mathbf{q},j}^* M_{\mathbf{q},l}, \tag{4}$$

where

$$M_{\mathbf{q},j} = \exp(\mathrm{i}\mathbf{q}.\mathbf{r}_j) \tag{5}$$

and c.c. represents the complex conjugate of the term preceding it. It will be noted that the LHS of (4) represents a difference between a measurable quantity $|F_{\mathbf{q}}^{\exp}|^2$ and a known one $|B_{\mathbf{q}}|^2$, while all quantities on the RHS are known, except for the surface electron distribution $\{u_j\}$. If the quantities $|F_{\mathbf{q}}^{\exp}|$ are measured for a sufficient number of different scattering vectors **q**, the resulting set of Eqs. (4) may be solved to recover that electron distribution [14].

In an earlier paper [16] we have pointed out a potential disadvantage of such an approach by an illustration with a test calculation to recover the (laterally averaged) variation, in a direction perpendicular to the surface of Ag(001), of the charge density of a K atom adsorbate at a height of 4.29 Å above the outermost substrate layer. This requires only the intensities of the $(00L)$ (specular) CTR, and a set of bulk diffracted amplitudes $B_{\mathbf{q}}$ for the same rod, which may be calculated, since the bulk structure is assumed known. For our test we simulated the "experimental" data, $|F^{\exp}_{00L}|$, using the ROD computer program of Vlieg [17]. We then recovered the electron distribution $\{u_j\}$ that minimizes the disagreement between the LHS and RHS of Eq. (4) by means of the APRIORI scheme of Saldin et al. [18], which employs repeated applications of a linear programming algorithm [19], to solve the non-linear equations (4). The progress of the recovery may be monitored by calculating the X-ray R-factor, R1 [1], quantifying the degree of agreement between the "experimental" data and a simulation of it from the recovered electron distribution. The iterations were halted when R1 reached about 0.06, an excellent R-factor by any standards. The resulting electron distribution had a spiky unphysical appearance, which did not much resemble a smooth distribution expected of the real electron density despite a near-perfect R-factor.

This was a graphic illustration of the thesis that in the presence of limited data, it is counter productive to overfit a model to the data. The problem is akin to taking the Fourier transform of a windowed function. The transform would be a convolution of the true electron distribution with that of the window. Of course the problem is exacerbated in the presence of noise since an exact solution of Eqs. (4) would fit not only the data, but also the noise. As we showed in our earlier paper [16], an approach based on Bayesian methods of statistical inference was able to much better reconstruct the true electron distribution, by balancing the need to minimize the R-factor with prior statistical considerations on the nature of the expected form of the electron distribution. We begin with a more detailed discussion of that theory.

4. Conditional probabilities and Bayes' theorem

A calculation of the probability of an event depends on a knowledge of factors that might determine that event. For example, at a location that has on average 100 rainy days in the year, *in the absence of any other knowledge*, one would say that the probability of rain on any given day was $100/365$. If however it was a spring day, and one knew that every other day in spring was rainy, one would instead estimate the probability of rain on that same day to be $1/2$. This gives rise to the concept of a conditional probability, $\mathrm{prob}(X|I)$ denoting the probability of proposition X given the validity of proposition I.

Two important rules follow from such a definition. The first is known as the *sum rule*:

$$\mathrm{prob}(X|I) + \mathrm{prob}(\overline{X}|I) = 1, \tag{6}$$

where $\overline{X}$ denotes that the proposition X is false. As an illustration, suppose I is the proposition that today is the 15th of May and that X is the proposition that it will rain on that day. The sum rule is thus a statement that the probability that it will rain and the mutually exclusive proposition that it will not rain on the 15th of May must sum to unity.

The *product rule* may be written

$$\mathrm{prob}(X, Y|I) = \mathrm{prob}(X|Y, I) \times \mathrm{prob}(Y|I). \tag{7}$$

In the context of the above analogy, suppose that Y is the proposition that there are clouds overhead. The product rule thus suggests that the product of the (independent) probability of overhead clouds on the 15th of May and the probability that it is raining when cloudy overhead on the 15th of May is equal to the probability that it is simultaneously rainy and cloudy overhead on that date.

Clearly the equation with X and Y interchanged must also be true by a similar argument. That is:

$$\mathrm{prob}(Y, X|I) = \mathrm{prob}(Y|X, I) \times \mathrm{prob}(X|I). \tag{8}$$

So far all equations represent common sense. A less obvious result follows from recognizing that the probabilities on the LHSs of the last two equations must be equal, and that therefore the RHSs may be equated. Doing this and dividing both sides by $\mathrm{prob}(Y|I)$ one obtains

$$\mathrm{prob}(X|Y, I) = \frac{\mathrm{prob}(Y|X, I) \times \mathrm{prob}(X|I)}{\mathrm{prob}(Y|I)}. \tag{9}$$

This non-trivial result is known as Bayes' theorem. In the case of our analogy, it relates the probability prob$(X|Y, I)$ that it rains when cloudy overhead on a particular day to the probability prob$(Y|X, I)$ that it is cloudy overhead when raining on that day. Everyday experience tells us that the latter probability is essentially unity, while the former may be quite small. Bayes' theorem [20] suggests how a knowledge of one may allow a calculation of the other.

The practical significance of this rather abstract discussion for a problem in X-ray crystallography may be seen if we identify the proposition X above with the electron density distribution, ρ, to be recovered from a set of measured diffraction "data", identified with Y above. Then we can write:

$$\text{prob}(\rho|\text{“data”}, I) = \frac{\text{prob}(\text{“data”}|\rho, I) \times \text{prob}(\rho|I)}{\text{prob}(\text{“data”}|I)}. \tag{10}$$

The LHS of the above equation may be regarded as the *posterior probability* of the electron density given the experimental data and background information. The first term in the numerator on the RHS is known as the *likelihood function* of the data for a given model of the electron density and the background information, and the second term in the numerator the *prior probability* of the electron density given the background information only. The denominator on the RHS is known as the *evidence*. For our problem the last-named quantity may be taken as constant, implying that all measured data is to be treated on an equal footing, and not biased by any background information. Eq. (10) then reduces to:

$$\text{prob}(\rho|\text{“data”}, I) \propto \text{prob}(\text{“data”}|\rho, I) \times \text{prob}(\rho|I). \tag{11}$$

The probability in the LHS of the above proportionality is what is sought in X-ray crystallography, and the above expression indicates that it is proportional to the product of the likelihood function and the prior probability.

In the context of X-ray crystallography, prob$(\text{“data”}|\rho, I)$ is the probability that a particular electron density model reproduces the measured intensities, a quantity that is usually estimated by conventional trial-and-error methods. The quantity on the LHS, prob$(\rho|\text{“data”}, I)$, the probability of a particular electron density for a given data set, is the quantity actually sought in crystallography. Eq. (11) shows how one may calculate one from the other together with a knowledge of the prior probability.

In the next two subsections we show how to calculate the likelihood function and the prior probability in the case of X-ray crystallography. The quantity of interest, namely the most probable electron density consistent with the measured diffraction data and any background information, may then be found by maximizing the functional formed by the product of the two probabilities on the RHS of (11).

4.1. Likelihood function

The likelihood function may be determined by the following argument: given an estimate σ_g of the standard deviation of the error in the experimental measurement of a structure factor amplitude $F_{\mathbf{q}}^{\text{exp}}$, the probability of such a measurement for a given model of the structure with calculated amplitude $F_{\mathbf{q}}^{\text{calc}}$ is given by the Gaussian distribution:

$$\text{prob}\big(F_{\mathbf{q}}^{\text{exp}}|\rho, I\big) = \frac{1}{\sigma_{\mathbf{q}}\sqrt{2\pi}} \exp\left\{-\frac{|F_{\mathbf{q}}^{\text{exp}} - F_{\mathbf{q}}^{\text{calc}}|^2}{2\sigma_{\mathbf{q}}^2}\right\}. \tag{12}$$

Given the multiplicative nature of independent probabilities, it follows that the likelihood function for the entire set of measured data is given by:

$$\text{prob}(\text{“data”}|\rho, I) = \text{prob}\big(\{F_{\mathbf{q}}^{\text{exp}}\}|\rho, I\big) \propto \exp\left\{-\frac{\chi^2}{2}\right\}, \tag{13}$$

where

$$\chi^2 = \sum_{\mathbf{q}} \frac{|F_{\mathbf{q}}^{\text{exp}} - F_{\mathbf{q}}^{\text{calc}}|^2}{\sigma_{\mathbf{q}}^2}. \tag{14}$$

This "chi-squared statistic" [20] could be regarded as another form of R-factor. The modulus of $F_{\mathbf{q}}^{\text{exp}}$ is the square root of the measured intensity. From the definition of the standard deviation $\sigma_{\mathbf{q}}$, the minimum expected value is of χ^2 would be of the order of the number of terms in the sum (14).

Eq. (13) shows that minimization of this R-factor is equivalent to maximizing the likelihood function. Eq. (11) shows, although this may be the standard

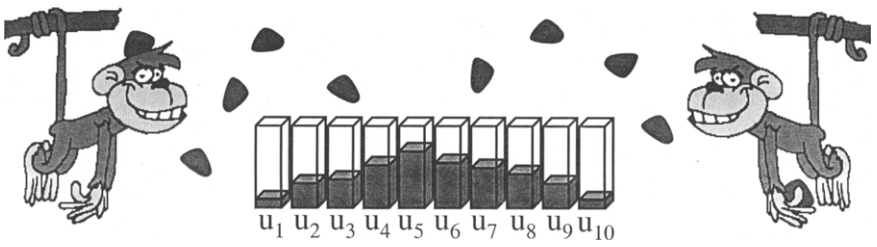

Fig. 2. The random filling of bins $\{1, 2, 3, \ldots\}$ of specified relative sizes $\{m_1, m_2, m_3, \ldots\}$ by a team of monkeys to produce a distribution $\{u_1, u_2, u_3, \ldots\}$ of objects.

practice in conventional trial-and-error structure determinations, the R-factor is only one element in the correct determination of a structure from a given set of measured data. It is necessary also to take account of the prior probability, as we will now show.

4.2. Prior probability

The prior probability of the electron distribution is simply the probability of the distribution given the background information, which is, in this case, just the positivity of the electron density and any prior estimate of that distribution on, e.g., chemical grounds. Any known periodicity allows attention to be confined to the electron distribution within a repeat unit (or unit cell). The *a priori* probability of such a distribution is analogous to the probability $P(u|I)$ that a hypothetical team of monkeys (our archetypal unbiased individuals, see Fig. 2) throw objects at random into a set of boxes $1, 2, 3, \ldots$ of capacities $m_1, m_2, m_3, \ldots$ to produce a distribution, $u_1, u_2, u_3, \ldots$, of those objects (where I now includes the information about the capacities of the boxes).

From the standard combinatorial argument,

$$\text{prob}\big(\{u_i\}|I\big) \propto \Omega = \prod_i m_i^{u_i} \Big/ \prod_i u_i!, \tag{15}$$

where Ω is the number of ways the distribution may come about. From Boltzmann's relation, the entropy, S, of the distribution may be written

$$S = \alpha \ln(\Omega), \tag{16}$$

where α is a constant. Combining Eqs. (15) and (16), we may write the prior probability as

$$\text{prob}\big(\{u_i\}|I\big) \propto \exp(S/\alpha). \tag{17}$$

In the crystallographic application, the quantities u_i are identified with the number of electrons in voxel (or "volume pixel") associated with a point i of a uniform grid within a unit cell. Thus the distribution $\{u\}$ is proportional to the electron density $\{\rho\}$ that crystallographers seek to determine. The distribution $\{m\}$ may be regarded as a prior estimate of $\{u\}$ based on the background information alone. For example, in protein crystallography, if the general shape of the molecule is known to low resolution, e.g., through a previously determined *solvent mask*, that knowledge may be incorporated into $\{m\}$.

4.3. Posterior probability

Combining Eqs. (11), (13), and (17), we find that the posterior probability may be written as

$$\text{prob}\big(\{u_i\}|\text{"data"}, I\big) \propto \exp\left(\frac{S}{\alpha} - \frac{1}{2}\chi^2\right). \tag{18}$$

5. Maximum entropy method

The most likely electron density distribution consistent with the experimental data and the background information is thus that which maximizes the exponent on the RHS of (18), or equivalently (since α is arbitrary), the functional, $Q[\{u_i\}]$, where:

$$Q\big[\{u_i\}\big] = \frac{S[\{u_i\}]}{\alpha} - \frac{\lambda}{2}\chi^2\big[\{u_i\}\big]. \tag{19}$$

Regarding λ as a Lagrange multiplier, we see that the problem of finding the most likely electron density consistent with the data may be reduced to that of finding the distribution of maximum entropy constrained by the requirement of minimizing the "chi-squared"

statistic. This is exactly the procedure of the maximum entropy method (MEM) of Jaynes [21].

The MEM has been applied to the problem of improving the initial "experimental" estimate of a set of phases of Bragg reflections in macromolecular crystallography by Collins [22]. There have been several subsequent applications of the MEM in this field (for a recent review, see Gilmore [23]). We present here an application of this method to surface X-ray diffraction (SXRD).

From Eqs. (15) and (16), and using Stirling's approximation:

$$\ln(u!) = u\ln(u) - u, \tag{20}$$

the entropy term in (19) may be written as

$$\frac{S}{\alpha} = -\sum_i u_i \ln(u_i/\mathrm{e}m_i) \tag{21}$$

where e is the base of natural logarithms. Writing

$$F_{\mathbf{q}}^{\mathrm{calc}} = B_{\mathbf{q}} + \sum_i u_i \exp(\mathrm{i}\mathbf{q}.\mathbf{r}_i) \tag{22}$$

substituting (22), (21), and (14) into (19), and taking $\sigma_{\mathbf{q}} = 1$ for all $\mathbf{q}$ (for theoretical "data") yields

$$\begin{aligned} Q\big[\{u_i\}\big] &= -\sum_i u_i \ln\left(\frac{u_i}{\mathrm{e}m_i}\right) - \frac{\lambda}{2}\sum_{\mathbf{q}}\Big|\,|F_{\mathbf{q}}^{\mathrm{exp}}|\exp(\mathrm{i}\phi_{\mathbf{q}}) \\ &\quad - B_{\mathbf{q}} - \sum_i u_i \exp(\mathrm{i}\mathbf{q}.\mathbf{r}_i)\Big|^2, \end{aligned} \tag{23}$$

where $\phi_{\mathbf{q}}$ is the phase of the measured structure factor $F_{\mathbf{q}}^{\mathrm{exp}}$. According to the theory developed above, the most probable electron distribution consistent with the experimental data $|F_{\mathbf{q}}^{\mathrm{exp}}|$ is that which maximizes the functional Q. We will derive an iterative algorithm for determining this distribution by writing the nth estimate of this distribution as $\{u_i^{(n)}\}$ and identifying $\{m_i\}$ with its estimate $\{u_i^{(n-1)}\}$ at the previous iteration. Thus we re-write (23) as

$$\begin{aligned} Q\big[\{u_i^{(n)}\}\big] &= -\sum_i u_i^{(n)} \ln\left(\frac{u_i^{(n)}}{\mathrm{e}u_i^{(n-1)}}\right)\cdots \\ &\quad - \frac{\lambda}{2}\sum_{\mathbf{q}}\Big|\,|F_{\mathbf{q}}^{\mathrm{exp}}|\exp(\mathrm{i}\phi_{\mathbf{q}}^{(n-1)}) \\ &\quad - B_{\mathbf{q}} - \sum_i u_i^{(n)} \exp(\mathrm{i}\mathbf{q}.\mathbf{r}_i)\Big|^2, \end{aligned} \tag{24}$$

where for $n > 1$

$$\phi_{\mathbf{q}}^{(n-1)} = \arg\left(B_{\mathbf{q}} + \sum_i u_i^{(n-1)} \exp(\mathrm{i}\mathbf{q}.\mathbf{r}_i)\right). \tag{25}$$

The distribution $\{u_i^{(n)}\}$ that maximizes Q is obtained by setting

$$\begin{aligned} \frac{\partial}{\partial u_i^{(n)}} Q\big[\{u_i^{(n)}\}\big] &= -\ln\left(\frac{u_i^{(n)}}{u_i^{(n-1)}}\right) - \lambda\big(t_i^{(n-1)} - u_i^{(n)}\big) \\ &= 0, \end{aligned} \tag{26}$$

for all i, where

$$t_i^{(n-1)} = \frac{1}{N}\sum_{\mathbf{q}}\big\{|F_{\mathbf{q}}^{\mathrm{exp}}|\exp(\mathrm{i}\phi_{\mathbf{q}}^{(n-1)}) - B_{\mathbf{q}}\big\}\exp(\mathrm{i}\mathbf{q}.\mathbf{r}_i) \tag{27}$$

and the sum over $\mathbf{q}$ includes Friedel pairs to ensure that $t_i^{(n-1)}$ is real. Eq. (26) may be re-written

$$u_i^{(n)} = u_i^{(n-1)} \exp\big\{-\lambda(u_i^{(n)} - t_i^{(n-1)})\big\} \tag{28}$$

which is an *implicit* equation for $u_i^{(n)}$. This can be converted into an explicit recursion relation for the same quantity by replacing $u_i^{(n)}$ on the RHS by $u_i^{(n-1)}$. This is justified if λ is chosen small enough that

$$\delta u_i^{(n)} \ll \big|u_i^{(n)} - t_i^{(n-1)}\big|, \tag{29}$$

where

$$\delta u_i^{(n)} = u_i^{(n)} - u_i^{(n-1)}. \tag{30}$$

Note that if λ were small enough it would be possible also to truncate the series expansion of the exponential on the RHS of (28) to approximate this equation by

$$\delta u_i^{(n)} = -\lambda u_i^{(n-1)}\big\{u_i^{(n)} - t_i^{(n-1)}\big\} \tag{31}$$

from which it follows that condition (29) is equivalent to the requirement that

$$\big|\lambda u_i^{(n-1)}\big| \ll 1 \tag{32}$$

which can be ensured by choosing

$$\lambda \ll 1/u_{\mathrm{max}}^{(n-1)}, \tag{33}$$

where $u_{\mathrm{max}}^{(n-1)}$ is the maximum value of the distribution $\{u_i^{(n-1)}\}$. Thus (28) may be replaced by the *explicit* recursion relation

$$u_i^{(n)} = u_i^{(n-1)} \exp\big\{-\lambda(u_i^{(n-1)} - t_i^{(n-1)})\big\} \tag{34}$$

so long as λ is chosen to satisfy (33).

A similar algorithm was proposed by Collins [22] for the related problem of improving the "experimental" phases in protein structure determination. It has been extended to the problem of protein structure completion by Saldin et al. [11,12], which is formally equivalent to the surface structure determination problem discussed here. The reason is that the diffracted amplitudes, e.g., $F_{\mathbf{q}}^{\exp}$, in surface crystallography are always a sum of a contribution $B_{\mathbf{q}}$ from a known bulk, and an unknown contribution, to be determined, from the surface.

It will be noted that the "target function" (27) has the form expected of the surface electron density: it consists of the difference between the total diffracted amplitude from the surface and that from the bulk. The only unknowns are the phases $\{\phi_{\mathbf{q}}\}$ of the measured data. An initial estimate of the target function $\{t_i^{(0)}\}$ requires initial estimates of the phases $\{\phi_{\mathbf{q}}^{(0)}\}$. We have found that an adequate estimate of this initial phase is the argument of the amplitude from a surface represented by a truncated bulk structure. That is we take

$$\phi_{\mathbf{q}}^{(0)} = \arg(B_{\mathbf{q}}). \tag{35}$$

As for $\{u_i^{(0)}\}$, following Collins [22], we take this to be same as $\{t_i^{(0)}\}$ except that, to ensure positivity, we replace all values of the distribution which are less than 1/100th of the maximum value $t_{\max}$ of the latter distribution (including all unphysical negative values) by $t_{\max}/100$. Substitution of these distributions in the RHS of (34) enables the evaluation of the next estimate $\{u_i^{(1)}\}$ of the surface electron distribution. Values of the phases $\{\phi_{\mathbf{q}}^{(n)}\}$ for $n > 0$ are estimated by Eq. (25).

Eqs. (25), (27) and (34) represent a set of recursion relations. The process is begun with an initial estimate of the phases of the measured diffraction amplitudes in reciprocal space. A Fourier transform yields the initial real-space target function $\{t_i\}$, which, in turn, is used to produce the next estimate of the electron distribution $\{u_i\}$. An inverse Fourier transform then returns an improved estimate of the phases $\{\phi_{\mathbf{q}}\}$. In terms of its repeated oscillation between real and reciprocal space this procedure has something in common with the Gerchberg–Saxton algorithm [24], which is also used for recovering phases from a real-space amplitude distribution. In reciprocal space the total diffracted amplitudes are kept at their experimentally determined values. In real space the electron distribution may be confined to its estimated physical bounds. The imposition of these restrictions at each iteration is one feature that enables the algorithm to successively improve its estimate of the unknown crystallographic phases.

6. Results

We describe below a couple of tests of this algorithm for the recovery of a 3D surface electron density of a couple of model surfaces from realistic simulations of surface X-ray diffraction from them, and a knowledge of the X-ray scattering amplitudes and phases from their known bulk structures. In both cases, the model surface structures have previously been determined by conventional diffraction methods, and so represent realistic surface structures.

6.1. O/Cu(104)

Our first example is the O/Cu(104) surface whose structure has earlier been determined by conventional surface X-ray diffraction methods [25]. In order to test our algorithm, we calculated by an adaptation of Vlieg's surface X-ray diffraction program [17] the intensities of the crystal truncation rods expected from that structure. A slice through reciprocal space parallel to the surface will intersect these CTRs at the set of points characterized by the H and K Miller indices shown in Fig. 3. The centered (2×2) surface unit cell restricts the combination of H and K Miller indices specifying a CTR to those with even values of $(H + K)$. Furthermore, due to the mirror planes perpendicular to the surface and parallel to the H-axis, it is necessary to measure only intensities of the rods with positive values of K. For the purposes of our test we simulated the intensities of just those 26 of these inequivalent CTRs shown in Fig. 3 for positive values of the Miller index L varying from 0 to 5.64 in intervals of 0.47. The combination of the mirror symmetry and Friedel's Law allowed us to deduce the intensities of all other CTRs shown in Fig. 3 for both positive and negative L. The additional data required of our algorithm are of course calculated values of the amplitudes and phases of the corresponding structure factors of the assumed unreconstructed bulk structure

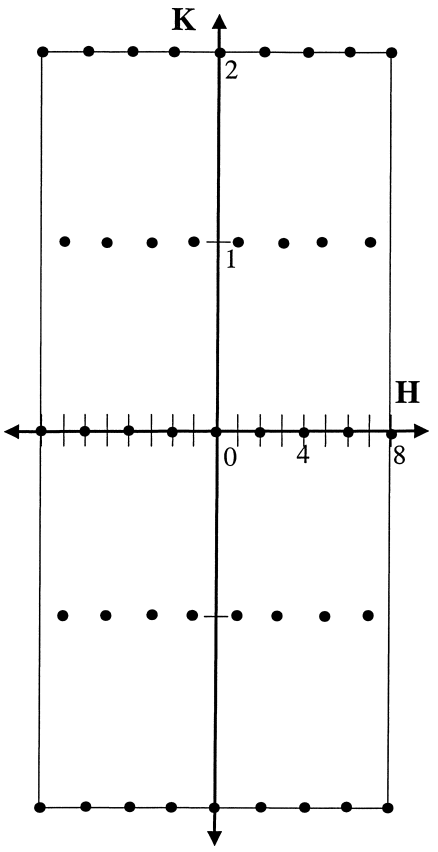

Fig. 3. Cut through reciprocal space parallel to the surface intersecting the crystal truncation rods (CTRs) from a Cu(104) surface. There is a mirror plane of symmetry perpendicular to the paper and passing through the H-axis. The diagram indicates all CTRs employed in the calculations.

of Cu(104). This was also calculated by the same computer program.

Fig. 4 shows a perspective view of a surface of constant electron density (an isosurface) of the initial estimate $\{u_i^{(0)}\}$ of the sought distribution. The larger light-colored spheres represent the assumed positions of the surface Cu atoms, while the smaller dark spheres indicate the positions of the adsorbate O atoms. The initial electron density appears to be peaked around the Cu atoms with little indication of the O atoms. Fig. 5 shows the surface electron distribution after about 1000 iterations of Eq. (34). Not only does the electron density around the O atoms now show up, but also that around the Cu substrate atoms appears more accurately centered around their true atom positions.

6.2. GaAs(111)-(2×2)

A potentially tougher test is the recovery of the electron density of the outermost two double layers of the GaAs(111)-(2×2) surface [26]. A conventional LEED analysis [27] has established that this surface reconstructs into the so-called vacancy buckling structure, in which there is not only a large relaxation and reconstruction of the outermost bilayer, but there is also a vacancy formed in this layer at the corners of a (2×2) surface unit cell. Fig. 6 shows a similar cut through reciprocal space parallel to the surface, which now intersects both the CTRs indexed by integer values of the H and K "in-plane" Miller indices of the substrate 2D reciprocal lattice, and also the reciprocal-space diffraction rods characterized by fractional values of ei-

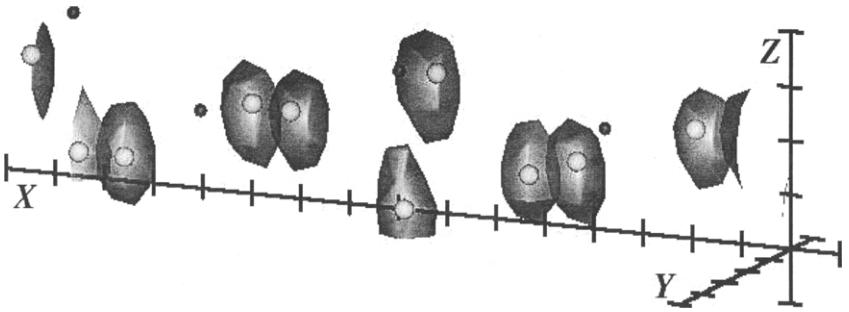

Fig. 4. Perspective view of isosurfaces of electron density representing the starting electron distribution $\{u_0\}$ of the O/Cu(104) surface unit cell. Note that the high-density regions enclose only the substrate Cu atoms (indicated by the larger light-colored dots). No significant electron density is found in the vicinity of the O adsorbate atoms (represented by the smaller, darker dots).

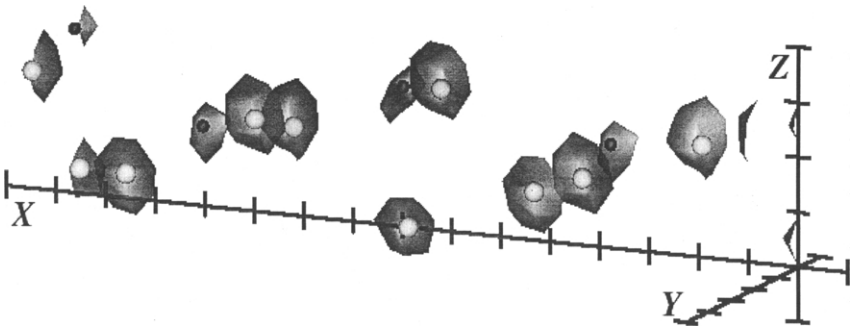

Fig. 5. Electron density isosurfaces in the same unit cell at the conclusion of the iterative algorithm. Note that now high electron density lobes are better centered around the Cu substrate atoms, and that they now also surround the O adsorbate atoms, thus revealing their positions.

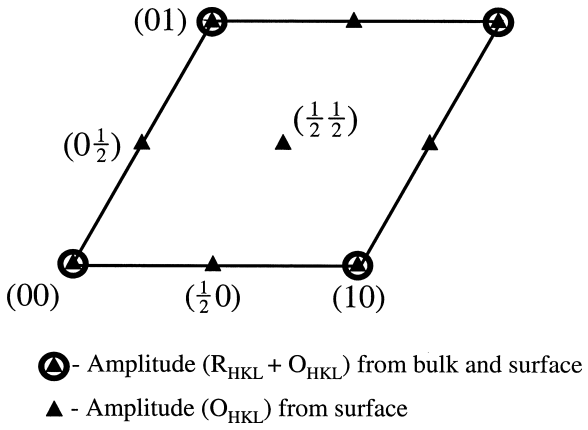

Fig. 6. Cut through reciprocal space parallel to the surface intersecting the crystal truncation rods (CTRs) specified by integer values of (HK) Miller indices, and superstructure rods corresponding to fractional values of either H or K.

ther index. The latter, which arise purely due to scattering by the (2×2) surface unit cell are known a *superstructure* rods. In contrast, the CTRs have contributions from both surface and bulk scattering, as in the case of our previous example.

Thus only the CTRs may be initially phased with reference to the bulk phases. Our strategy for dealing with this case is to begin by allowing the algorithm to operate on just the CTR data. The resulting surface electron density distribution will have a (1×1) periodicity which is the average of the density of each of the (1×1) quadrants of the true (2×2) periodicity. The starting distribution $\{u_i^{(0)}\}$ of the outermost two double layers of a (2×2) surface unit cell calculated from the initial assignment of the phases of the bulk to $\{\phi_{\mathbf{q}}\}$ (followed by truncation of the negative values of $\{t_i^{(0)}\}$ as described previously) is shown in perspective in Fig. 7. Diffraction data from all rods with values of $|H|, |K| \leqslant 2$ were used in this calculation. (Fig. 6 indicates only the rods in the 1st Brillouin zone of the 2D reciprocal lattice of the bulk.) The small spheres shown in Fig. 6 mark the positions of the surface atoms in the model, with the lighter-colored ones representing As atoms and the darker ones the Ga. One feature of the vacancy buckling model is that although the spacing of the lower double layer remains at approximately its bulk value, the uppermost double layer relaxes so as to make the two components of that double layer almost co-planar.

The electron density isosurfaces in Fig. 7 obviously have a (1×1) 2D periodicity. The isosurfaces also appear to be consistent with an extension of the bulk structure in each of the outermost two double layers, where the relaxation of the outermost double layer is not apparent. However, this relaxation is recovered after 1000 iterations of the recursion relation (34). The distribution $\{u_i^{(n)}\}$ illustrated in Fig. 8 shows almost co-planar isosurfaces associated with the Ga and As atoms in the outermost double layer, although naturally the (1×1) periodicity of the average structure remains.

The recovery of the true (2×2) periodicity of the surface requires the inclusion also of data from the superstructure (or fractional-order) rods. At this point the Fourier summation for the target function (27) is taken to include the amplitudes from the fractional-order rods. As for their initial phases, these are those

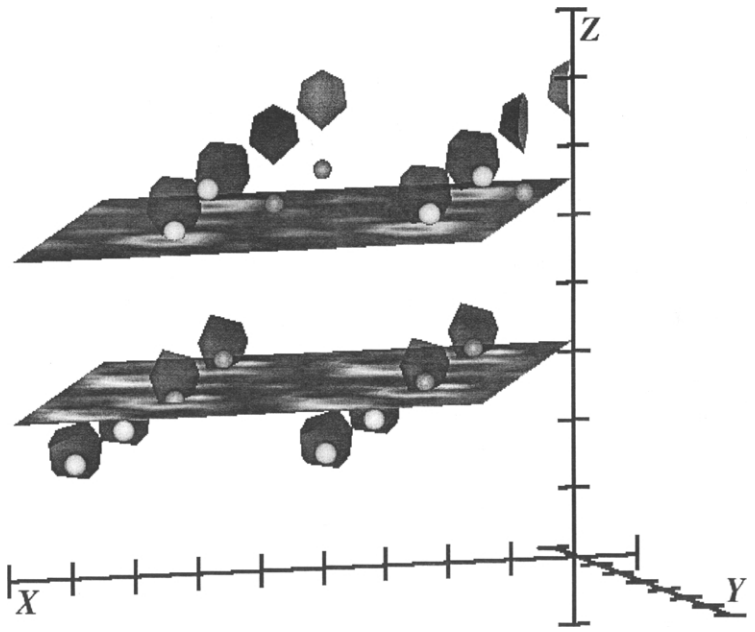

Fig. 7. Perspective view of high electron density isosurfaces of the starting distribution $\{u_0\}$ of the outer two double layers of a GaAs(111)-(2×2) surface unit cell. The larger, light colored dots represent positions of As atoms in the vacancy-buckling model, while the smaller, darker dots denote the corresponding positions of the Ga atoms. Note that the isosurfaces signify positions of atoms in a bulk-terminated surface (with no relaxation or reconstruction) with distinct double layers. The x-y planes indicate the approximate level of each of the two outermost double layers of the surface. The shading within each of these planes represents the variation of the electron density within that plane.

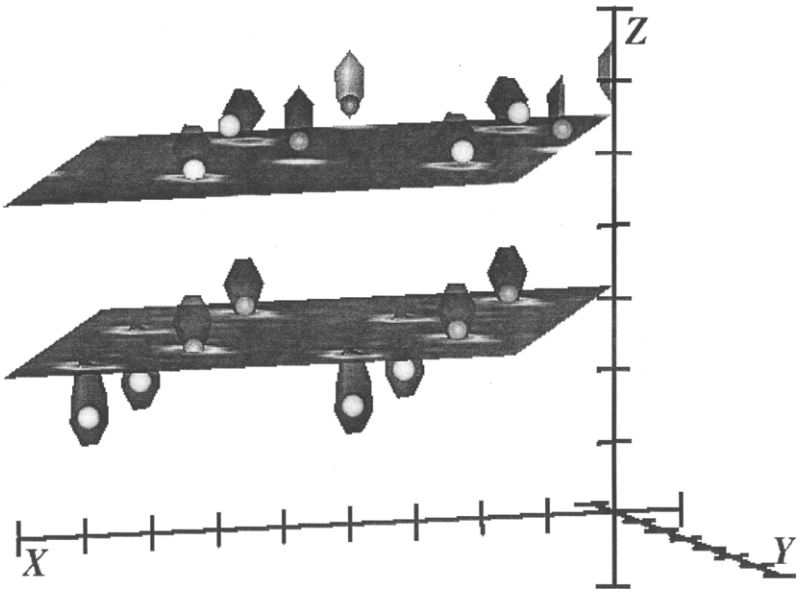

Fig. 8. High electron density isosurfaces after modification of the density distribution of Fig. 7 by the inclusion of just the (integer-order) CTRs in the iterative algorithm. Note that the isosurface lobes in the upper double layer indicate the relaxation of this layer to produce almost co-planar As and Ga atoms. Note, however, that the isosurfaces indicate a (1×1) periodicity parallel to the surface.

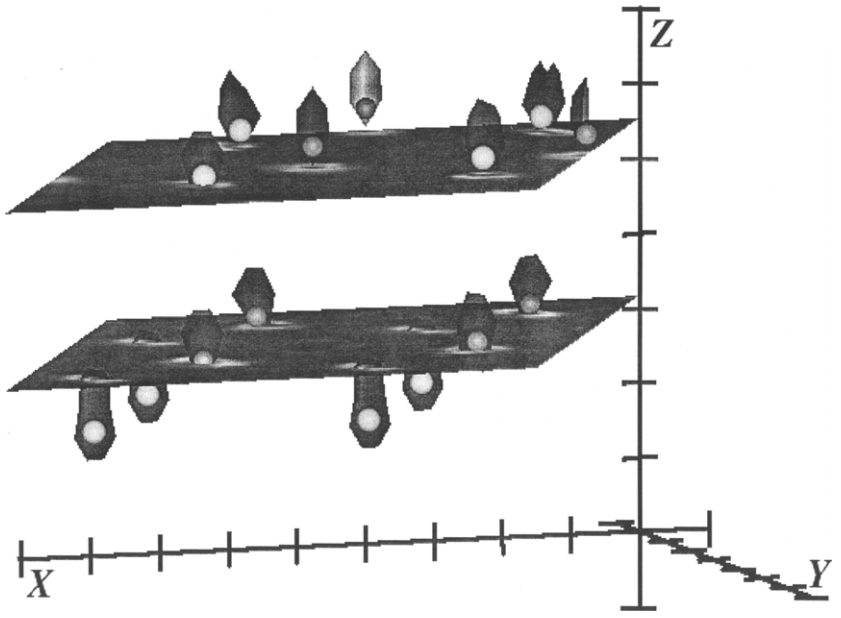

Fig. 9. Final high density isosurfaces recovered after the inclusion of both the CTRs and the (fractional-order) superstructure rods in the iterative algorithm. The true (2×2) periodicity of the outermost double layer is now recovered with no high electron density in the vicinity of the vacancy at the z-axis in the outermost double layer. Note that the isosurfaces now surround just the model atom positions in this complicated reconstructed surface.

found from interpolating from the current estimates of the phases of their neighboring (integer-order) CTRs. The resulting surface electron distribution after 1000 further iterations of (34) is shown in Fig. 9. These isosurfaces are seen to accurately pinpoint the locations of all atoms in the vacancy buckling model. It correctly reproduces the (2×2) 2D periodicity and even shows up the vacancy at the corners of the (2×2) unit cell.

7. Discussion and conclusions

With the advent of a new generation of synchrotron radiation sources, surface X-ray diffraction is emerging as one of the most attractive methods for surface crystallography. The relatively weak scattering of X-rays from a surface allows the diffracted amplitude to be written as a Fourier transform of the surface electron density. In turn, this opens up the prospect of developing a method for directly recovering the electron density of an entire surface unit cell from measured SXRD intensities and a knowledge of the bulk structure.

In this paper we have described and applied such a method to calculate SXRD data from realistic model structures containing adsorbates and substantial surface reconstructions. In each case the electron density of the entire surface unit cell was accurately recovered. The method proposed is closely analogous to holography. The ensemble of measurable SXRD intensities may be regarded as constituting a hologram. They consist of the square modulus of a sum of the structure factor from the known bulk unit cell, which may be regarded as a reference wave, and the structure factor of the unknown surface unit cell, which may be regarded as an object wave to be determined. We discuss possible holographic reconstruction algorithms to recover this object wave, or equivalently by Fourier transformation, the electron density of the entire surface unit cell.

In particular we develop an algorithm based on ideas of Bayesian statistics in general, and the maximum entropy principle in particular. Such an algo-

rithm balances the need to fit incomplete (and possibly noisy) data with other requirements based on prior statistical knowledge about the nature of the electron distribution sought. The effectiveness of the algorithm is illustrated with test calculations on simulated data from the realistic surface structures of O/Cu(104) and GaAs(111)-(2×2).

Acknowledgements

DKS and IKR acknowledge support for this work from the U.S. National Science Foundation (Grant Nos. DMR-9815092 and DMR-9876610, respectively).

References

[1] M.A. Van Hove, W.H. Weinberg, C.-M. Chan, Low-Energy Electron Diffraction, Springer, Berlin, 1986.
[2] J.B. Pendry, K. Heinz, W. Oed, Phys. Rev. Lett. 61 (1988) 2953.
[3] A. Szöke, in: D.J. Attwood, J. Boker (Eds.), Short Wavelength Coherent Radiation: Generation and Applications, AIP Conference Proceedings, Vol. 147, American Institute of Physics, New York, 1986.
[4] D. Gabor, Nature (London) 161 (1948) 777.
[5] R.J. Collier, C.B. Burckhardt, L.H. Lin, Optical Holography, Academic Press, New York, 1971.
[6] J.J. Barton, Phys. Rev. Lett. 61 (1988) 1356.
[7] D.K. Saldin, P.L. De Andres, Phys. Rev. Lett. 64 (1990) 1270.
[8] M. Tegze, G. Faigel, Nature 380 (1996) 49.
[9] T. Gog, P.M. Len, G. Materlik, D. Bahr, C.S. Fadley, C. Sanchez-Hanke, Phys. Rev. Lett. 76 (1996) 3132.
[10] K. Reuter, J. Bernhardt, H. Wedler, J. Schardt, U. Starke, K. Heinz, Phys. Rev. Lett. 79 (1997) 4818.
[11] D.K. Saldin, V.L. Shneerson, D.L. Wild, J. Imaging Sci. Technol. 41 (1997) 482.
[12] V.L. Shneerson, D.L. Wild, D.K. Saldin, Acta Cryst. A 51 (2001) 163.
[13] I.K. Robinson, Phys. Rev. B 33 (1986) 3830.
[14] A. Szöke, Phys. Rev. B 47 (1993) 14 044.
[15] A. Szöke, Acta Cryst. A 49 (1993) 853.
[16] D.K. Saldin, R. Harder, V.L. Shneerson, H. Vogler, W. Moritz, in: M. Benfatto, C.R. Natoli, E. Pace (Eds.), Theory and Computation for Synchrotron Radiation Spectroscopy, AIP Conference Proceedings, Vol. 514, American Institute of Physics, New York, 2000, p. 130.
[17] E. Vlieg, J. Appl. Cryst. 33 (2000) 401.
[18] D.K. Saldin, X. Chen, N. Kothari, M.H. Patel, Phys. Rev. Lett. 70 (1993) 1112.
[19] D.G. Luenberger, Introduction to Linear and Nonlinear Programming, Addison-Wesley, Reading, MA, 1973.
[20] D.S. Sivia, Data Analysis: A Bayesian Tutorial, Oxford University Press, Oxford, 1996.
[21] E.T. Jaynes, Phys. Rev. 106 (1957) 620.
[22] D.M. Collins, Nature 298 (1982) 49.
[23] C.J. Gilmore, Acta Cryst. A 52 (1996) 561.
[24] R.W. Gerchberg, W.O. Saxton, Optik 35 (1972) 237.
[25] D.A. Walko, I.K. Robinson, Surf. Rev. Lett. 6 (1999) 851.
[26] This is a repeat of an earlier calculation on the very similar InSb(111)-(2×2) structure (which also reconstructs to a vacancy buckling structure) by two of us (H. Vogler, W. Moritz, unpublished).
[27] S.Y. Tong, W.N. Mei, G. Xu, J. Vac. Sci. Technol. B 2 (1984) 393.